18

Raman Spectroscopy of CNC- and CNF-Based Nanocomposites

Umesh P. Agarwal

US Forest Service, Forest Products Laboratory, 1 Gifford Pinchot Drive, Madison, WI 53726, USA

Abstract

In this chapter, applications of Raman spectroscopy to nanocelluloses and nanocellulose composites are reviewed, and it is shown how use of various techniques in Raman can provide unique information. Some of the most important uses consisted of identification of cellulose nanomaterials, estimation of cellulose crystallinity, study of dispersion of cellulose nanocrystals (CNCs) in polymers, and assessment of CNC/matrix interactions. Further, using a bleached fiber, it was demonstrated that information on the orientation of cellulose at the molecular level can be obtained with the help of polarized Raman spectroscopy. This capability can therefore be used to study the organization of nanocelluloses in composites. Lastly, in nanocellulose composites, an example was given of how Raman spectroscopy can be used to quantify the strain or stress transferred to nanocelluloses from the surrounding polymer matrix.

Keywords *Raman spectroscopy; nanocellulose; nanocomposite; cellulose nanocrystal; cellulose nanofibril*

List of Abbreviations

CNC	cellulose nanocrystal
CNF	cellulose nanofibril
CrI	crystallinity index
EV	electric vector
FT	Fourier transform
IR	infrared
MAPP	maleated polypropylene
MCC	microcrystalline cellulose
NMR	nuclear magnetic resonance
PP	polypropylene
PVA	polyvinyl alcohol

Handbook of Nanocellulose and Cellulose Nanocomposites, First Edition.
Edited by Hanieh Kargarzadeh, Ishak Ahmad, Sabu Thomas, and Alain Dufresne.

SCNF short cellulose nanofibril
S/N signal-to-noise
TERS tip-enhanced Raman spectroscopy
WAXS wise-angle X-ray scattering
XRD X-ray diffraction

18.1 Introduction

Raman spectroscopy is a powerful nondestructive technique to investigate cellulose materials. Technological developments in the field of Raman in terms of filters, detectors, and lasers have made Raman spectrometers more suited to investigations of cellulose materials. Over the years, along with the advances in Raman instrumentation, new capabilities were developed in a number of areas. Besides development of new sampling methods to analyze nanocelluloses in the never dried state (author's unpublished information), these included estimation of cellulose crystallinity [1], measurement of water accessibility of celluloses at the molecular level [2], and determination of mechanical properties of celluloses [3]. This chapter reviews Raman studies of cellulose nanocrystals (CNCs), cellulose nanofibrils (CNFs), and their composites. Although nanocellulose materials have been investigated only recently by the technique, Raman spectroscopy – along with its subtechniques, has been used for a long time in the field of celluloses and their products. In the context of a nanocellulose composite, its Raman spectrum gives molecular-level information on each of the constituents, which in itself is unique information. However, Raman is capable of much more. This technique can be used to determine crystallinity of cellulose nanoparticles, investigate their distribution in polymers (using Raman mapping), and evaluate nanocellulose interactions with the matrix. Chemical mapping [4] is a powerful technique which detects and images chemicals with high sensitivity. The Raman spectra of nanocelluloses can also be used to measure the strain or stress transferred to them from the surrounding matrix and to examine local stresses and strains in nanocomposites. Therefore, Raman spectroscopy has great potential in the characterization of the structure of nanocomposites and the quantitative measurements of physical properties. Among the many different applications, this chapter focuses on structural analysis, presence of mixed phases, cellulose crystallinity, chemical mapping, and tensile deformation.

18.2 Raman Spectroscopy

Raman spectroscopy is based on the Raman effect, which results from interactions of the vibrational modes of molecules with electromagnetic radiation. However, this effect is quite weak; approximately one out of a million photons is Raman scattered (inelastic scattering). In a Raman spectrum, vibrational frequencies are measured relative to the excitation frequency, and the signal intensity is proportional to $1/\lambda^4$, where λ is the excitation wavelength. Because of this relationship between the intensity and wavelength, it is appealing to use

a short-wavelength laser. However, it is important to remember that sample autofluorescence generated at low wavelengths can easily degrade S/N ratio and thereby make Raman bands difficult to detect. In celluloses and lignocelluloses, the presence of a small amount of impurities [5] or lignin [6] can create the problem of autofluorescence. This is the primary reason for using excitation in the 633–1064 nm region. For a large number of celluloses, excitation at 1064 nm (near infrared (IR)) mostly eliminates autofluorescence [7]. However, it also reduces the Raman signal intensity. For this reason, to compensate for this disadvantage, Fourier transform (FT)-Raman instruments are used [7, 8]. In FT instruments, in contrast to the conventional grating-based dispersive instrument (ultraviolet and visible Raman), advantage is taken of the high-throughput characteristic of the interferometer [8]. Nevertheless, in either case, the Raman shifts are directly related to the functional group and the structure of the molecule to which the group is attached. Moreover, the Raman frequency also depends upon the types of atoms in the molecule and molecular environment. Using Raman spectroscopy, identification of materials in a multicomponent system can be simply accomplished. Additionally, using polarized Raman, orientation of nanocelluloses in polymer matrices or within all-cellulose samples can be carried out.

18.3 Micro-Raman and Raman Imaging

In a micro-Raman experiment, an optical microscope in combination with spectrometer is used [9, 10]. This allows acquisition of Raman spectra of a microscopic sample (e.g., single fibers) or microscopic domains in a solid sample. Not only is much less sample required, but, in cases where confocal sampling is used [4, 11], autofluorescence can be suppressed because the fluorescence from regions outside of the confocal area is not detected. Some examples of micro-Raman applications include studies of cellulose fibers and composites [3, 4, 12, 13].

In the case of Raman imaging or mapping, the spatial distribution of a component can be obtained in two dimensions with the help of a Raman microscope [4, 11]. Obviously, this kind of information is useful in a heterogeneous sample. Although the laser spot size is diffraction limited, the mapping yields information on the local composition of the sample at high spatial resolution. For example, a number of researchers have used Raman imaging [4, 14, 15] to investigate woody tissue, and the distribution of both lignin and cellulose was mapped simultaneously by selecting Raman bands that are specific to these cell wall components. This methodology has been used in our investigations of nanocellulose composites as well (see more in the following text).

18.4 Applications to Cellulose Materials

18.4.1 Celluloses

Although CNCs and CNFs are new materials in the field of cellulose science [16], other celluloses and cellulose-based products have been around for a long time,

and Raman as an analytical technique has been applied to their investigations. Earlier work dealt with topics such as band assignments [13], cellulose structure [17] and orientation [13, 18], and polymorphism [19] in celluloses. Over the years, the field of Raman spectroscopy has continued to evolve and has made significant technological advances especially in terms of instrumentation [20]. This has benefited studies of celluloses because the developments allowed acquisition of spectra with high S/N ratio and reduced level of fluorescence [6, 7]. In addition to fluorescence suppression, the availability of near-IR FT-Raman instruments made possible the acquisition of low-frequency (50–250 cm^{-1}) spectra [21]. This is the region where vibrational modes due to H bonds and crystals are usually detected [22, 23]. In 2010, to estimate cellulose crystallinity, a new method based on 380 cm^{-1} band of cellulose was published [1]. The method ranked high when compared, using a number of criteria, to Segal-WAXS and ^{13}C NMR [24]. To assess crystallinity, the Raman method, also known as "380-Raman," has been applied to a wide variety of cellulose materials including CNCs and CNFs [1, 25–30]. Some of the novel Raman applications consist of information on local CH_2OH conformation, accessibility of water to cellulose at the molecular level, and information on the H bonds [2, 7].

Additionally, tensile uniaxial tests in Raman spectroscopy have been used to investigate deformation mechanisms of stand-alone cellulose fibers as well as of wood, paper, and cellulose nanocomposites [31–37]. It was reported that, in the spectrum of cellulose, the shifts of the 1095 cm^{-1} band give information on the molecular deformation of the material, which is related to the stress within the fiber. Using this shift, Young's modulus of bacterial cellulose fibril was predicted from the calibration of the Raman shift at 1995 cm^{-1} against modulus [33]. Therefore, Raman spectroscopy plays an important role in understanding the micromechanics of nanocellulose and its composites. This capability can generate information that is useful in understanding the variability in mechanical behavior of various nanocellulose composites.

18.4.2 CNCs and CNFs

18.4.2.1 Spectra

Raman spectra of nanocelluloses produced from different sources have been obtained in the author's laboratory. Since nanocelluloses do not have distinctive Raman spectra, the technique cannot be used to prove the existence of nanocelluloses. However, the Raman frequency, intensity, and band shape of the vibrations can vary between the celluloses and nanocelluloses. In general, the spectral features (band intensities and profiles) differ within the same family of nanocelluloses (e.g., within CNCs) or between the two types of nanocelluloses (e.g., CNCs vs. CNFs). Nevertheless, in most cases, the spectrum of a nanocellulose is similar to the spectrum of the cellulose material from which it was generated (author's unpublished work). Figure 18.1 shows spectra of CNCs in their dry state. The spectra are plotted after being normalized at 1096 cm^{-1} (one of many bands of cellulose). Although a large number of spectral features are similar, there are significant differences as well. Between spectra, small differences exist with regard to Raman frequencies, band profiles, and band

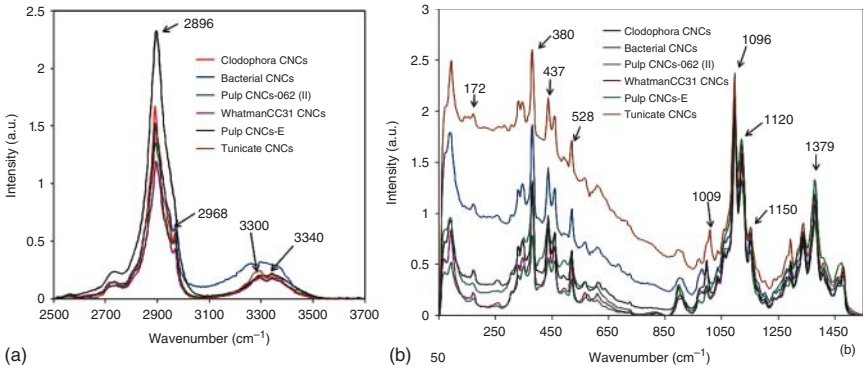

Figure 18.1 (a) Raman spectra of various CNCs in 2500–3700 cm^{-1} region showing contributions of C–H and O–H stretches and (b) Raman spectra of various CNCs in 50–1500 cm^{-1} region. The CNCs with sharper and stronger features are indicative of higher crystallinity.

intensities. In most cases, the highest intensities are associated with highly crystalline CNCs (e.g., spectra of those derived from tunicate and cladophora). On contrary, pulp-derived CNCs (samples CNCs-E and CNCs-062 (II)) show lower intensity peaks, and their crystallinity is significantly lower compared with that derived from tunicate. Moreover, in the spectra of the CNC produced from a dissolving grade of bleached kraft pulp that contained cellulose II (CNCs-062 (II)), have spectral features indicating the presence of cellulose II (e.g., 577 and 1462 cm^{-1} bands [7, 19]).

As an example of the differences between the CNCs and CNFs (both devoid of any cellulose II), spectra of the two types of wood pulp nanocelluloses are shown in Figure 18.2. Raman frequencies of these CNCs and CNFs are compared in Table 18.1. The nanocelluloses used in this work were generated from bleached hardwood kraft pulps.

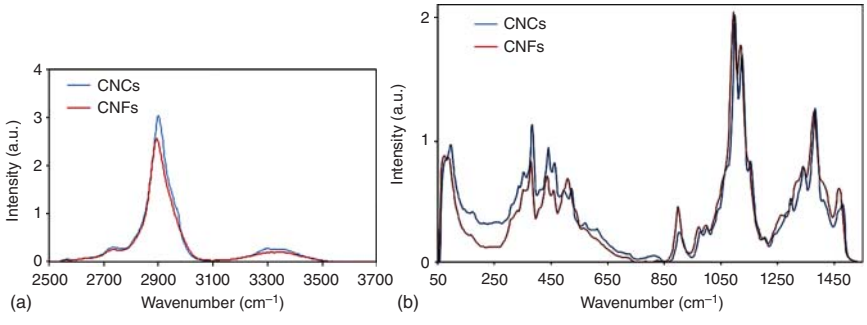

Figure 18.2 (a) Raman spectra of wood pulp CNCs and CNFs in 2500–3700 cm^{-1} region showing contributions of C–H and O–H stretches and (b) Raman spectra of wood pulp CNCs and CNFs in 50–1500 cm^{-1} region. CNCs have comparatively better resolved features partly due to removal of residual hemicelluloses.

Table 18.1 Comparison of Raman frequencies of pulp-CNCs and pulp-CNFs (cm^{-1}).

Pulp-CNCs	Pulp-CNFs	Pulp-CNCs	Pulp-CNFs
3347 (m[a])	3341 (m)	974 (w-m)	971 (w-m)
3298 (m)	3301 (m)	913 (sh)	—
2967 (sh)	—	900 (m-s)	898 (m-s)
2934 (sh)	—	817 (vw)	—
2893 (vs)	2894 (vs)	724 (sh)	—
2816 (sh)	—	609 (vw)	609 (vw)
2734 (sh)	2733 (sh)	566 (sh)	567 (vw)
2716 (sh)	—	—	534 (sh)
1478 (sh)	—	520 (m)	520 (sh)
1462 (sh)	1467 (m-s)	—	509 (m)
1407 (m)	1416 (sh)	492 (w)	495(sh)
1380 (s)	1379 (s)	460 (m)	460 (m)
1338 (m)	1340 (w-m)	437 (m)	436(m)
—	1315 (sh)	408 (sh)	408 (sh)
1293 (w)	1294 (w)	380 (s)	380 (s)
1277 (sh)	1263 (sh)	350 (m)	352 (w)
1236 (w)	—	333 (sh)	331 (sh)
1202 (w)	1202 (w)	307 (sh)	309 (sh)
1148 (m)	1148 (sh)	210 (vvw)	210 (vvw)
1121 (s)	1120 (s)	171 (w)	168 (w)
1097 (vs)	1095 (vs)	154 (vw)	—
1066 (sh)	1058 (sh)	139 (vw)	—
1037 (sh)	—	92 (m)	93 (sh)
997 (w-m)	997 (w-m)		

a) Relative band intensity in the spectrum; vs, very strong; s, strong; m, medium; w, weak; vw, very weak; vvw, very very weak; sh shoulder.

Considering that Raman spectral features can vary depending upon the interaction with other components or molecules, such variations can be used to obtain information about the nature, localization, and force of the interaction. This is particularly useful in the case of composites where the CNCs and CNFs are embedded in polymer matrix.

Between the spectra of the CNCs and CNFs, one of the important points to remember is the sharpness of the peaks in the spectrum of the CNCs (Table 18.1 and Figure 18.2). This is due to two reasons – CNCs having higher crystallinity and removal of hemicelluloses from CNCs upon acid hydrolysis. Raman contributions of hemicelluloses have been reported previously [7, 38]. Contributions of xylan [7, 38] were detected at 1120 and 495 cm^{-1} (Table 18.1 and Figure 18.2b).This is supported by Figure 18.2b where, for CNFs, the 1120 cm^{-1} band was more intense and less resolved (red) compared with that of the CNCs (blue).

18.4.2.2 Crystallinity

Crystallinity is one of many important structural properties of nanocelluloses, and Raman spectroscopy has been used to estimate their crystallinity[1, 24–30]. In such measurements, the ratio of cellulose's Raman bands at 380 and 1096 is used [1]. Based on the application of the 380-Raman method thus far, this method has proven to be reliable in most cases as long as proper correction for hemicellulose or syringyl lignin is carried out [25]. In the present situation, comparing the 1096 cm^{-1} normalized spectra shown in Figure 18.2b, the existence of the stronger 380 cm^{-1} peak for CNCs implies that these are more crystalline compared with the CNFs. However, considering that hemicelluloses also contributed at 1096 cm^{-1} but not at 380 cm^{-1}, a correction for their presence needs to be performed. This can be easily carried out by using the calibration curve that already exists [25]. Nonetheless, one needs to know the amount of hemicelluloses present in a sample. 380-Raman is not the only cellulose crystallinity measurement method where such issues need to be addressed. Other methods (e.g., X-ray and ^{13}C NMR) have been found to have similar limitations when estimating crystallinity of nanocelluloses and their composites. And more importantly, some of these issues may be the reasons why results of crystallinity measurements by different researchers have been, at times, contradictory [39, 40].

Table 18.2 lists Segal-WAXS and 380-Raman crystallinities of a large[1] number of CNCs that were produced by acid hydrolysis under a variety of conditions

Table 18.2 CNC crystallinities (CrI) determined by Segal-WAXS and 380-Raman methods.

ID	CNCs sample[a)] (acid concentration, temperature, time)	CrI–Raman (I_{380}/I_{1096})	CrI–Segal-WAXS
1	(56, 70, 90) 10-5	55.4	74.3 ± 0.0
2	(58, 56, 60) 14-1	48.4	73.6 ± 0.4
3	(58, 56, 120) 14-3	50.4	72.8 ± 0.5
4	(58, 56, 180) 14-5	57.0	75.5 ± 0.7
5	(58, 56, 210) 14-6	50.0	73.4 ± 2.1
6	(62, 40, 75) 7-4	51.8	78.5 ± 0.1
7	(62, 40, 105) 7-6	50.2	77.4 ± 0.5
8	(62, 50, 60) 4-3	50.3	75.4 ± 0.1
9	(62, 50, 75) 4-4	51.4	76.0 ± 0.6
10	(62, 60, 30) 1-1	51.8	73.4 ± 0.0
11	(62, 60, 60) 1-3	53.6	76.1 ± 0.5
12	**(64, 45, 15) 13-0**	**39.8**	**68.5 ± 1.3**
13	(64, 45, 45) 13-2	54.0	72.0 ± 0.2
14	(64, 45, 75) 13-4	54.4	73.9 ± 1.7
15	(64, 45, 105) 13-6	54.9	75.4 ± 0.1

a) See [30] for information on CNC samples.

1 Values in bold are the lowest crystallinity values.

where acid concentration, temperature, and time of hydrolysis were varied. This table is adapted from the publication of Chen *et al.* [30]. Although for sample 12 (data in bold) both the Raman and X-ray diffraction (XRD) methods gave lower crystallinity compared with other samples, further examination of the sample's Raman spectrum indicated that cellulose II was present in this CNC sample. Because cellulose II contributes to the band at 1096 cm^{-1} [7, 19] and has no contribution to the signal at 380 cm^{-1}, this makes the ratio (I_{380}/I_{1096}) lower. Since the estimated crystallinity is based on this ratio [1], the sample crystallinity would be lower compared with the other samples where cellulose II was not present (Table 18.2). This explained why the estimated Raman crystallinity of the sample was lower (Table 18.2). Examination of the X-ray diffractogram of the sample failed to bear this out, which is not surprising given that the presence of low levels of cellulose II is difficult to detect by X-ray.

18.4.2.3 Orientation

With the help of polarized Raman spectroscopy, orientation of nanocelluloses can be investigated. This approach is similar to examining the orientation of cellulose molecules in a fiber [13]. Although there are several bands in cellulose that show sensitivity to the way the cellulose molecules are oriented relative to the electric vector (EV) direction of the laser, most often, 1096 and 2900 cm^{-1} are used due to their high Raman intensity. Some of the recent examples where Raman spectroscopy has been used to investigate cellulose orientation are the works of Hsieh *et al.* [33], Zimmerley *et al.* [41], and Gierlinger *et al.* [42].

As an example of ability of Raman spectroscopy to provide information on cellulose orientation, a set of spectra are shown in Figure 18.3. These spectra were obtained from a cellulose fiber, and the Raman microprobe setup was such that Raman spectra could be obtained at different fiber-direction angles with respect to the EV of the laser. The fiber was rotated, on the microscope stage, between

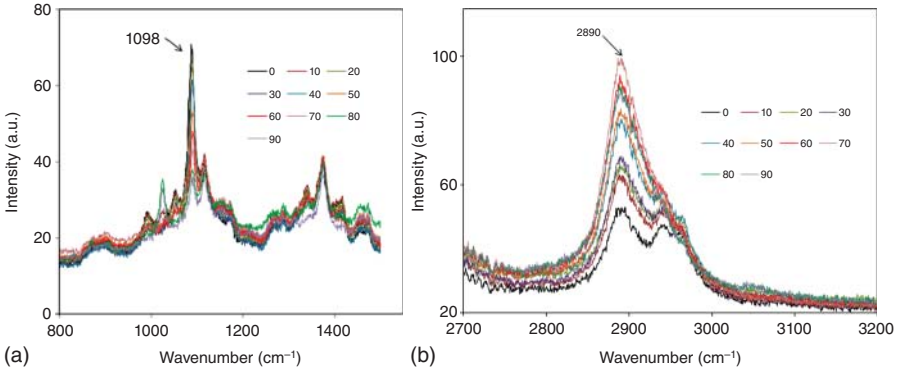

Figure 18.3 (a) Raman spectra of bleached kraft pulp fiber in the 800–1500 cm^{-1} region. Different spectra represent various orientations of the long fiber axis with respect to the EV direction of the laser (angle θ from 0° to 90°). At 1098 cm^{-1}, spectra show the presence of most and least intense peaks at θ being 0° and 90°, respectively. (b) Raman spectra of bleached kraft pulp fiber in 2700–3200 cm^{-1} region. Different spectra represent various orientations of the long fiber axis with respect to the EV direction of the laser. Spectra are shown at different values of θ.

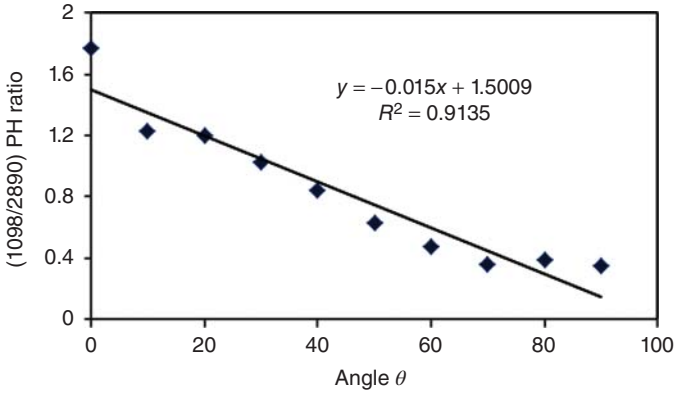

Figure 18.4 Correlation between the band intensity ratio (1098/2890) and angle θ (between long fiber axis and EV direction of the laser).

0° and 90°, by 10° and a spectrum was obtained from the same location every 10°. Thus, 10 spectra were obtained from the sampled area on the fiber in the two spectral regions (1098 and 2900 cm^{-1} regions). These regions represented the C–O and C–C and the C–H stretches in the cellulose molecule, respectively.

With the angle "θ" between the EV direction and the fiber direction being zero, the band at 1098 cm^{-1} showed the highest intensity (black spectrum in Figure 18.3a), and its intensity declined at higher θ angles. The minimum intensity was obtained at a θ value of 90°. The opposite trend was obtained in case of the C–H stretch mode (Figure 18.3b). This behavior of oriented cellulose is known and has been used to estimate the microfibril angle in the cell wall and in pulp fibers [42, 43]. In the author's laboratory, polarized Raman spectroscopy has been used to investigate orientation of wood and pulp fibers and, more recently, of nanocelluloses (unpublished work).

When the ratio of the peak height (PH) intensity of the bands at 1098 and 2890 cm^{-1} is plotted against θ, a linear correlation is obtained (Figure 18.4). This implies that to evaluate the angle between the fiber axis and the EV direction, one simply needs to take the ratio of the two intensities. However, in cases where only one of the band intensities is available, that information can also be used to estimate value of θ [13, 43]. Nevertheless, the ratio method has the advantage that no internal/external reference is required to monitor changes in the experimental variables or any fluctuations between the spectra are accounted for.

18.5 Applications to Nanocomposites

Considering that nanocellulose-based composites are biodegradable and environmentally friendly, they are desirable replacements for conventional composites based on petroleum feedstock. Nanocelluloses have been combined with various materials to produce composites with desirable properties [16, 44]. The celluloses are attractive structural components which serve as a mechanical reinforcement phase in composites. The presence of the CNCs and CNFs in a polymer matrix has the potential to not only stiffen the matrix but also increase its strength

depending on factors such as nanocellulose dispersion, the aspect ratio (length divided by width) of the nanocellulose, and the adhesion between the nanocellulose and matrix. In this section of the chapter, several applications of Raman spectroscopy to nanocellulose-based composite materials are reviewed.

18.5.1 CNCs

18.5.1.1 Mapping

Given that nanocellulose composites are inherently heterogeneous, both standard and spatially resolved Raman spectroscopies [7, 45] have been used to analyze them in our laboratory. One set of nanocomposites characterized were CNC–polypropylene (PP) composites wherein the spatial distribution of CNCs in extruded composite filaments [45] was studied. Three composites were made from two forms of nanocellulose (CNCs from wood pulp and the nanoscale fraction of microcrystalline cellulose (MCC)), and one of the three investigated composites contained maleated polypropylene (MAPP)which was used as a coupling agent. In Figure 18.5, 1064 nm FT-Raman spectra of PP (Figure 18.5a), 50/50 fractionated MCC/MAPP (Figure 18.5b), and acetylated CNC (Figure 18.5c) in the region 850–1550 cm^{-1} are shown. Compared to PP, cellulose signals were weaker, although the contributions at 1098 and 1120 cm^{-1} due to CNCs could be easily detected in the MCC/MAPP composite spectrum (Figure 18.5b).

The composites were also studied using 633 nm-based confocal Raman imaging [4]. The spectroscopic approach to investigating spatial distribution of the composite components was helpful in evaluating CNC dispersion in the composite at the microscopic level, which helped explain the relatively modest reinforcement of PP by the CNCs [45]. Raman maps based on cellulose and PP bands at 1098 and 1460 cm^{-1}, respectively, obtained at 0.6 μm spatial resolution showed

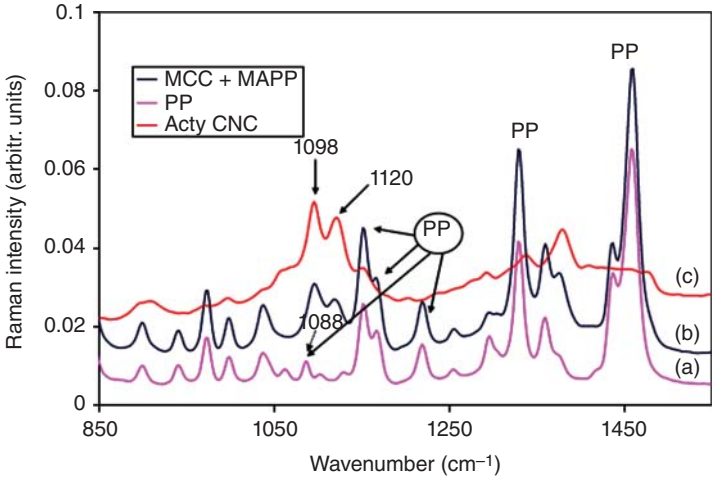

Figure 18.5 FT-Raman spectra of (a) PP, (b) 50/50 fractionated MCC/MAPP, and (c) acetylated CNC in the region 850–1550 cm^{-1}.

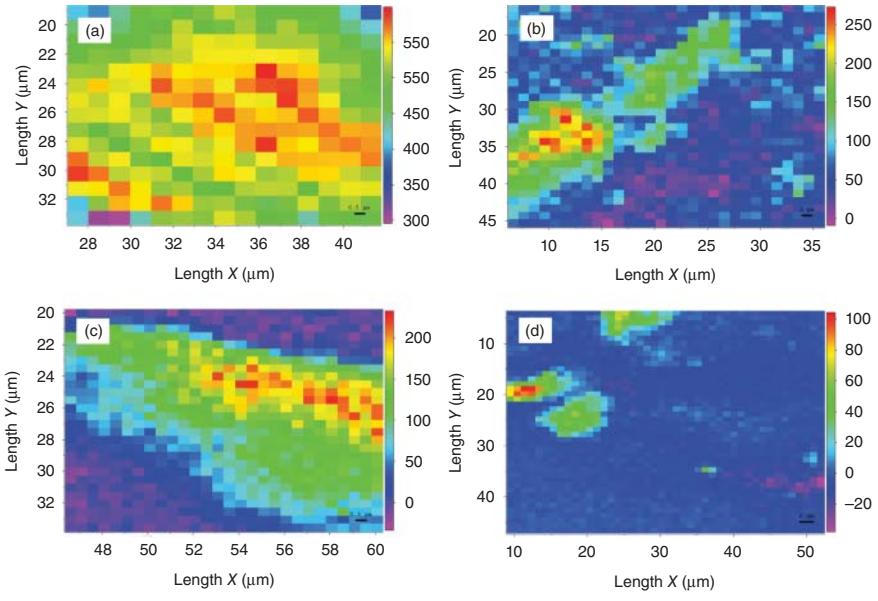

Figure 18.6 Raman images (false color) of spatial distributions of composite components: (a) PP in an unreinforced PP, (b) CNCs in PP with acetylated CNC, (c) CNCs in PP with fractionated MCC, and (d) CNCs in PP with CNC and MAPP. Note the different scale bar values in different images ((a), 0.5 μm; (b), 1 μm; (c), 0.5 μm; (d), 2 μm). The intensity scale for each Raman map appears on the right of the image. High, medium, and very low component concentrations are indicated as red, green, and blue regions, respectively. Some locations show negative values and arise from the manner in which intensities were calculated for the images. (Agarwal *et al*. 2012 [45]. Reproduced with permission of Sage Publications.)

that the CNCs were aggregated to various degrees in the PP matrix. Of the three composites analyzed, two showed clear existence of regions of poor dispersion: Raman images with strong PP and absent/weak cellulose or vice versa. For the third composite, the situation was slightly improved, but a clear transition interface between the PP-abundant and CNC-abundant regions was observed, indicating that the CNC remained poorly dispersed. Figure 18.6 shows Raman images of spatial dispersions of the two composite components.

18.5.1.2 Tensile Deformation

One of the important needs in nanocellulose composite research is to understand how stress from matrix is transferred to celluloses. In other words, what are the stress transfer mechanisms? Raman spectroscopy is able to provide information on deformation of both phases – nanocellulose and the matrix. The Raman band at 1095 cm^{-1} is known to shift under mechanical tension [31]. In the literature, a number of publications have used the strain-sensitive aspect of the Raman peak. For example, Rusli *et al.* [34] investigated tunicate CNC and poly(vinyl acetate) nanocomposites by polarized Raman spectroscopy and showed that the stress transfer was influenced by local orientation of the nanocrystals. Shifts of 1095 cm^{-1} Raman band as a result of uniaxial deformation of nanocomposite films were used to determine the degrees of stress experienced by the CNCs,

not only due to stress transfer from the matrix to the tunicate CNCs but also between the CNCs within the composite. In a more recent publication, Pullawan *et al.* [46] studied the deformation micromechanics of all-cellulose nanocomposites by Raman spectroscopy. Four different nanocomposites were created from cotton and tunicate CNCs using two different cellulose matrices. Stress transfer mechanisms between the matrix and the CNCs in these composites are reported by following the molecular deformation of both the CNCs and matrix celluloses – cellulose I and cellulose II, respectively. Such a study allowed the authors to draw important conclusions on what is required to obtain maximum tensile strength and modulus.

18.5.2 CNFs

18.5.2.1 Tensile Deformation

A system that used short cellulose nanofibril (SCNF) as reinforcement in polyvinyl alcohol (PVA) fiber is reported in [37]. Composite fibers were produced by adding SCNFs to PVA fibers. The molecular orientation of PVA was affected by a combination of wet drawing during gel spinning and hot drawing at a high temperature after drying. Peng *et al.* [37] reported that the strength and modulus of PVA/SCNF composite fiber with a SCNF weight ratio of 6 were nearly 60% and 220% higher than that of PVA by itself.

Raman spectra of PVA, PVA/SCNF6 filaments, and SCNF cast film are shown in Figure 18.7. The cellulose band at 1095 cm^{-1} is present in the spectra. As shown in Figure 18.8, shifts in the Raman peak at 1095 cm^{-1} indicated good stress transfer between the SCNF and the PVA matrix due to strong interfacial hydrogen

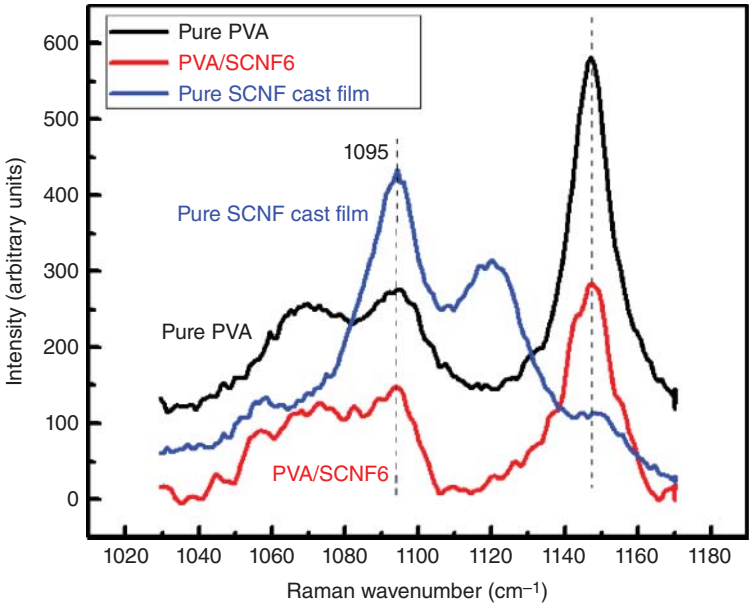

Figure 18.7 Typical Raman spectra in region 1020–1180 cm^{-1}, PVA, PVA/SCNF6 (drawn filaments), and SCNF cast film highlighting the Raman peak initially located at 1095 cm^{-1}.

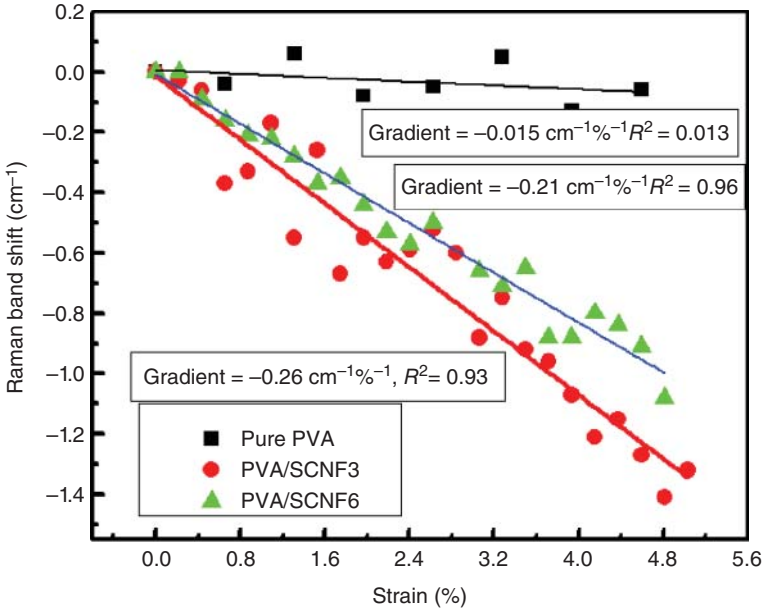

Figure 18.8 Shifts in 1095 cm^{-1} Raman band upon tensile deformation for pure PVA, PVA/SCNF3, and PVA/SCNF6 drawn fiber with a draw ratio of 27. Solid lines are linear regressions for the data.

bonding and were responsible for increases in the strength and modulus of the fibers.

It is clear from these examples that, in a nanocellulose composite, Raman shift in the 1095 cm^{-1} band can serve as sensor to detect the elastic stress or strain in the polymer matrix and reinforcement. Such information may be useful not only to evaluate distribution of stress but also to detect or predict the onset of failure in composite materials.

18.5.3 Future Developments

It is going to be speculative to tell what the future is going to bring to the field of Raman applications to the nanocomposites. From the instrumentation point of view, the need to carry out nanometer-resolved Raman spectroscopy on celluloses and the composites is one of the most important desires of the researchers that is not being met by the existing instrumentation. The analysis capability at the nano level, although realized for a number of noncellulose materials via tip-enhanced Raman spectroscopy (TERS) [47], has emerged as a candidate for desirable future development. If and when that happens, Raman imaging experiments will become possible at the level of single cellulose molecule. On other fronts, of course, given that Raman inherently suffers from the problem of sensitivity, efforts will continue to be made to address this topic. Additionally, development of new lasers with circular beam profiles, especially in the near-IR range, is needed. The near-IR range is the excitation wavelength region where a compromise exists between availability of good detectors and low

autofluorescence of samples. Considering that some nanocellulose composites fluoresce even at 1064 nm, even longer-wavelength lasers would be desirable, but then detectors capable of sensitive detection of Raman scattering in the entire Raman range would be required. In addition to autofluorescence, use of Raman spectroscopy is not yet widespread because of the cost of Raman instrumentation, which happens to be still significantly higher compared with its IR counterparts. Nevertheless, Raman is capable of much higher spatial resolution. The cost factor can be expected to change given that progressively more research institutions and laboratories are going to acquire Raman capability.

18.6 Summary

A review of Raman spectroscopy applications to nanocelluloses and nanocellulose-based composites was provided, and various capabilities of the technique were highlighted. It was shown that Raman can be used not only to identify cellulose nanomaterials and estimate cellulose crystallinity but also to study the dispersion of CNCs in polymers and assess CNC–matrix interactions. Using a bleached fiber, it was shown that the polarized Raman spectra provided information on the orientation of cellulose at the molecular level and that this capability can also be used to study the organization of nanocelluloses. Moreover, in a CNC composite, Raman spectroscopy can be used to quantify the strain or stress transferred to CNCs from the surrounding polymer matrix. This ability of Raman which is based on the shift of the 1095 cm^{-1} band allowed investigation of local stresses and strains in cellulose composite materials.

Acknowledgments

The author is grateful to Dr. Craig Clemons for providing Figures 18.7 and 18.8 used in the manuscript. He would also like to acknowledge the help of Rick Reiner and Sally Ralph for obtaining some of Raman data reported here.

References

1 Agarwal, U.P., Reiner, R.S., and Ralph, S.A. (2010) Cellulose I crystallinity determination using FT–Raman spectroscopy: univariate and multivariate methods. *Cellulose*, **17**, 721–733.
2 Agarwal, U.P., Ralph, S.A., Reiner, R.S., and Baez, C. (2016) Probing crystallinity of never-dried wood cellulose by Raman spectroscopy. *Cellulose*, **23** (1), 125–144.
3 Sturcova, A., Davies, G.R., and Eichhorn, S.J. (2005) Elastic modulus and stress-transfer properties of tunicate cellulose whiskers. *Biomacromolecules*, **6**, 1055–1061.
4 Agarwal, U.P. (2006) Raman imaging to investigate ultrastructure and composition of plant cell walls: distribution of lignin and cellulose in black spruce wood (*Picea mariana*). *Planta*, **224**, 1141–1153.

5 Atalla, R.H. and Nagel, S.C. (1972) Laser-induced fluorescence in cellulose. *J. Chem. Soc., Chem. Commun.*, 1049–1050.
6 Agarwal, U.P. (1999) in *Advances in Lignocellulosics Characterization* (ed. D.S. Argyropoulos), TAPPI Press, Atlanta, pp. 201–225.
7 Agarwal, U.P. (2014) 1064 nm FT-Raman spectroscopy for investigations of plant cell walls and other biomass materials. *Front. Plant Sci.*, **5**, 490.
8 Hendra, P., Jones, C., and Warnes, G. (eds) (1991) *Fourier Transform Raman Spectroscopy: Instrumentation and Chemical Applications*, Ellis Horwood Ltd, Chichester.
9 Atalla, R.H. and Agarwal, U.P. (1986) Recording Raman spectra from plant cell walls. *J. Raman Spectrosc.*, **17** (2), 229–231.
10 Turrell, G., Delhaye, M., and Dhamelincourt, P. (1996) in *Raman Microscopy: Developments and Applications* (eds G. Turrell and J. Corset), Academic Press, San Diego, CA, pp. 27–49.
11 Barbillat, J. (1996) in *Raman Microscopy: Developments and Applications* (eds G. Turrell and J. Corset), Academic Press, San Diego, CA, pp. 175–200.
12 Atalla, R.H. and Agarwal, U.P. (1985) Raman microprobe evidence for lignin orientation in the cell walls of native woody tissue. *Science*, **227**, 636–638.
13 Wiley, J.H. and Atalla, R.H. (1987) Band assignments in the Raman spectra of celluloses. *Carbohydr. Res.*, **160**, 113–129.
14 Gierlinger, N. and Schwanninger, M. (2006) Chemical imaging of poplar wood cell walls by confocal Raman microscopy. *Plant Physiol.*, **140** (4), 1246–1254.
15 Zhang, X., Ji, Z., Zhou, X., Ma, J.-F., Hu, Y.-H., and Xu, F. (2015) Method for automatically identifying spectra of different wood cell wall layers in Raman imaging data set. *Anal. Chem.*, **87**, 1344–1350.
16 Eichhorn, S.J., Dufresne, A., Aranguren, M., Marcovich, N.E., Capadona, J.R., Rowan, S.J., Weder, C., Thielemans, W., Roman, M., Renneckar, S., Gindl, W., Veigel, S., Keckes, J., Yano, H., Abe, K., Nogi, M., Nakagaito, A.N., Mangalam, A., Simonsen, J., Benight, A.S., Bismarck, A., Berglund, L.A., and Peijs, T. (2010) Review: current international research into cellulose nanofibres and nanocomposites. *J. Mater. Sci.*, **45** (1), 1–33.
17 Atalla, R.H., Rauna, J., and Malcolm, E.W. (1984) Raman spectroscopic studies of the structure of cellulose: a comparison of kraft and sulfite pulps. *Tappi J.*, **67** (2), 96–99.
18 Wiley, J.H. and Atalla, R.H. (1987) in *The Structures of Cellulose*, ACS Symposium Series, vol. **340** (ed. R.H. Atalla), ACS, Washington, DC, pp. 151–168.
19 Atalla, R.H. (1976) Raman spectral studies of polymorphy in cellulose. Part I – celluloses I and II. *Appl. Polym. Symp.*, **28**, 659–669.
20 Adar, F., Delhaye, M., and DaSilva, E. (2007) Evolution of instrumentation for detection of the Raman effect as driven by available technologies and by developing applications. *J. Chem. Educ.*, **84**, 50–60.
21 Colaianni, S.E.M. and Nielsen, O.F. (1995) Low-frequency Raman spectroscopy. *J. Mol. Struct.*, **347**, 267–284.
22 Colaianni, S.E.M., Aubard, J., Hansen, S.H., and Nielsen, O.F. (1995) Raman spectroscopic studies of some biochemically relevant molecules. *Vib. Spectrosc.*, **9**, 111–120.

23 Parrott, E.P.J., Zeitler, J.A., Friscic, T., Pepper, M., Jones, W., Day, G.M., and Gladden, L.F. (2009) Testing the sensitivity of terahertz spectroscopy to changes in molecular and supramolecular structure: a study of structurally similar cocrystals. *Cryst. Growth Des.*, **9**, 1452–1460.

24 Agarwal, U.P. (2015) Pros and cons of cellulose crystallinity estimation methods: 380-Raman, ^{13}C NMR, and Segal-WAXS. American Chemical Society, Division of Cellulose and Renewable Materials 249th ACS National Meeting, Denver, CO, Presentation # 63.

25 Agarwal, U.P., Reiner, R.S., and Ralph, S.A. (2013) Estimation of cellulose crystallinity of lignocelluloses using near-IR FT-Raman spectroscopy and comparison of the Raman and Segal-WAXS methods. *J. Agric. Food Chem.*, **61**, 103–113.

26 Qing, Y., Sabo, R., Zhu, J.Y., Agarwal, U.P., Cai, Z., and Wu, Y. (2013) A comparative study of cellulose nanofibrils disintegrated via multiple processing approaches. *Carbohydr. Polym.*, **97**, 226–234.

27 Agarwal, U.P., Reiner, R.S., and Ralph, S.A. (2014) in *Production and Applications of Cellulose Materials* (eds M.T. Postek, R.J. Moon, A.J. Rudie, and M.A. Bilodeau), TAPPI Press, Atlanta, pp. 43–44.

28 Agarwal, U.P., Zhu, J.Y., and Ralph, S.A. (2013) Enzymatic hydrolysis of loblolly pine: effects cellulose crystallinity and delignification. *Holzforschung*, **67**, 371–377.

29 Agarwal, U.P., Ralph, S.A., Reiner, R.S., Moore, R.K., and Baez, C. (2014) Impacts of fiber orientation and milling on observed crystallinity in jack pine. *Wood Sci. Technol.*, **48**, 1213–1227.

30 Chen, L., Wang, Q., Hirth, K., Baez, C., Agarwal, U.P., and Zhu, J.Y. (2015) Tailoring the yield and characteristics of wood cellulose nanocrystals (CNC) using concentrated acid hydrolysis. *Cellulose*, **22**, 1753–1762.

31 Eichhorn, S.J., Sirichaisit, J., and Young, R.J. (2001) Deformation mechanisms in cellulose fibers, paper and wood. *J. Mater. Sci.*, **36** (13), 3129–3135.

32 Šturcová, A., Davies, G.R., and Eichhorn, S.J. (2005) Elastic modulus and stress-transfer properties of tunicate cellulose whiskers. *Biomacromolecules*, **6** (2), 1055–1061.

33 Hsieh, Y.-C., Yano, H., Nogi, M., and Eichhorn, S.J. (2008) An estimation of the Young's modulus of bacterial cellulose filaments. *Cellulose*, **15** (4), 507–513.

34 Rusli, R., Shanmuganathan, K., Rowan, S.J., Weder, C., and Eichhorn, S.J. (2010) Stress-transfer in anisotropic and environmentally adaptive cellulose whisker nanocomposites. *Biomacromolecules*, **11** (3), 762–768.

35 Tanpichai, S., Sampson, W.W., and Eichhorn, S.J. (2014) Stress transfer in microfibrillated cellulose reinforced poly(vinyl alcohol) composites. *Composites Part A*, **65**, 186–191.

36 Gierlinger, N., Schwanninger, M., Reinecke, A., and Burgert, I. (2006) Molecular changes during tensile deformation of single wood fibers followed by Raman microscopy. *Biomacromolecules*, **7** (7), 2077–2081.

37 Peng, J., Ellingham, T., Sabo, R., Turng, L.-S., and Clemons, C.M. (2014) Short cellulose nanofibrils as reinforcement in polyvinyl alcohol fiber. *Cellulose*, **21**, 4287–4298.

38 Agarwal, U.P. and Ralph, S.A. (1997) FT-Raman spectroscopy of wood: identifying contributions of lignin and carbohydrate polymers in the spectrum of black spruce (*Picea mariana*). *Appl. Spectrosc.*, **51** (11), 1648–1655.

39 Iwamoto, S., Nakagaito, A.N., and Yano, H. (2007) Nano-fibrillation of pulp fibers for the processing of transparent nanocomposites. *Appl. Phys. A*, **89**, 461–466.

40 Abe, K. and Yano, H. (2010) Comparison of the characteristics of cellulose microfibril aggregates isolated from fiber and parenchyma cells of Moso bamboo (*Phyllostachys pubescens*). *Cellulose*, **17**, 271–277.

41 Zimmerley, M., Younger, R., Valenton, T., Oertel, D.C., Ward, J.L., and Potma, E.O. (2010) Molecular orientation in dry and hydrated cellulose fibers: a coherent anti-Stokes Raman scattering microscopy study. *J. Phys. Chem. B.*, **114**, 10200–10208.

42 Gierlinger, N., Luss, S., König, C., Konnerth, J., Eder, M., and Fratzl, P. (2010) Cellulose microfibril orientation of Picea abies and its variability at the micron-level determined by Raman imaging. *J. Exp. Bot.*, **61** (2), 587–595.

43 Pleasants, S., Batchelor, W.J., and Parker, I.H. (1998) Measuring the fibril angle of bleached fibers using micro-Raman spectroscopy. *Appita J.*, **51** (5), 373–376.

44 Moon, R.J., Martini, A., Nairn, J., Simonsen, J., and Youngblood, J. (2011) Cellulose nanomaterials review: structure, properties and nanocomposites. *Chem. Soc. Rev.*, **40** (7), 3941–3994.

45 Agarwal, U.P., Sabo, R., Reiner, R.S., Clemons, C.M., and Rudie, A.W. (2012) Spatially resolved characterization of cellulose nanocrystal-polypropylene composite by confocal Raman microscopy. *Appl. Spectrosc.*, **66** (7), 750–756.

46 Pullawan, T., Wilkinson, A.N., Zhang, L.N., and Eichhorn, S.J. (2014) Deformation micromechanics of all-cellulose nanocomposites: comparing matrix and reinforcing components. *Carbohydr. Polym.*, **100**, 31–39.

47 Schmid, T., Opilik, L., Blum, C., and Zenobi, R. (2013) Nanoscale chemical imaging using tip-enhanced Raman spectroscopy: a critical review. *Angew. Chem. Int. Ed.*, **52**, 5940–5954.